ifested itself in the context of NF-κB:IκB complexes and not free IκB proteins. We transfected hemagglutinin (HA)–tagged κB-Ras1, p65, IκBα, and IκBβ by themselves or in combination into COS cells (*31*). COS cells were used because they have extremely low amounts of NF-κB and related proteins, and hence only the transfected proteins are detected in immunoblotting assays. Cotransfected HA-tagged κB-Ras1 associated efficiently with coexpressed IκBβ but very poorly with coexpressed IκBα (Fig. 5C). Cotransfection of p65 along with κB-Ras1 and IκBα or IκBβ resulted in p65 being immunoprecipitated only with the κB-Ras–IκBβ complex (Fig. 5C). Thus, κB-Ras appears to associate only with p65-bound IκBβ protein in these overexpression experiments.

If the association of κB-Ras proteins with NF-κB:IκBβ complexes is mediated mainly through interaction with IκBβ, then degradation of IκBβ should lead to a loss of κB-Ras protein that can be immunoprecipitated with NF-κB. To test this hypothesis, we stimulated 293 cells with IL-1, an inducer that causes IκBβ degradation in about 90 min (Fig. 5D). Immunoblotting with an antibody to κB-Ras revealed that the amount of κB-Ras proteins was not altered upon stimulation (Fig. 5D). We then immunoprecipitated NF-κB p65 from the stimulated extracts, followed by immunoblotting of the immunoprecipitates with the κB-Ras antibody. The amount of coimmunoprecipitated κB-Ras decreased in a manner proportional with the decrease in IκBβ levels (Fig. 5E), consistent with the possibility that κB-Ras is anchored to the NF-κB:IκBβ complex through IκBβ.

The κB-Ras proteins specifically associate with PEST domains and influence their degradation. It is therefore possible that they might also regulate the turnover of other PEST domain–containing proteins besides IκBβ. In fact, we detected κB-Ras proteins in high–molecular weight complexes, distinct from the cytoplasmic NF-κB/IκB complexes (*22*). Identification of these other κB-Ras–associated proteins will therefore be crucial in understanding the overall biological role of κB-Ras proteins.

References and Notes

1. M. J. May and S. Ghosh, *Immunol. Today* **19**, 80 (1998).
2. J. L. Bos, *EMBO J.* **17**, 6776 (1998).
3. F. McCormick, *Curr. Opin. Genet. Dev.* **4**, 71 (1994).
4. J. L. Bos, *Mutat. Res.* **195**, 255 (1988).
5. _____, *Cancer Res.* **49**, 4682 (1989).
6. M. Barbacid, *Annu. Rev. Biochem.* **56**, 779 (1987).
7. B. M. Willumsen, A. Christensen, N. L. Hubbert, A. G. Papageorge, D. R. Lowy, *Nature* **310**, 583 (1984).
8. M. W. Mayo *et al.*, *Science* **278**, 1812 (1997).
9. R. Perona *et al.*, *Genes Dev.* **11**, 463 (1997).
10. S. Y. Na *et al.*, *J. Biol. Chem.* **273**, 3212 (1998).
11. C. Fenwick *et al.*, data not shown.
12. L. M. Facchini and L. Z. Penn, *FASEB J.* **12**, 633 (1998).
13. P. A. Lawrence, *Cell* **54**, 1 (1988).
14. I. G. Macara, K. M. Lounsbury, S. A. Richards, C. McKiernan, D. Bar-Sagi, *FASEB J.* **10**, 625 (1996).
15. A. Valencia, P. Chardin, A. Wittinghofer, C. Sander, *Biochemistry* **30**, 4637 (1991).
16. Construction of the phylogenic tree was done with the Phylip software package. The Ras similarity domains (corresponding to amino acids 5 to 164 of H-Ras) were aligned by ClustalW alignment and compared by parsimonious analysis with amino acid similarities and bootstrapping analysis. Although variations of the Ras family dendrogram were generated, κB-Ras1 and κB-Ras2 remained grouped with Ras/Ral/Rap proteins.
17. D. R. Lowy and B. M. Willumsen, *Annu. Rev. Biochem.* **62**, 851 (1993).
18. D. G. Winkler, J. C. Johnson, J. A. Cooper, A. B. Vojtek, *J. Biol. Chem.* **272**, 24402 (1997).
19. Nucleotide binding to κB-Ras1 was performed by slot-blot analysis with bacterially expressed κB-Ras1 with a COOH-terminal His tag. κB-Ras1 was purified on nickel-agarose gel and dialyzed extensively in a buffer containing 1 mM EDTA before the nucleotide-binding assay (*32*).
20. J. L. Bos, *Biochim. Biophys. Acta* **1333**, M19 (1997).
21. J. Cherfils *et al.*, *EMBO J.* **16**, 5582 (1997).
22. C. Fenwick and S. Ghosh, unpublished observations.
23. E. Kopp and S. Ghosh, *Science* **265**, 956 (1994).
24. For transfection studies, HeLa, 293, and Jurkat cells were seeded into 24-well plates (1×10^5 cells per well, 1×10^6 for Jurkat cells) and grown for 24 hours before transfection with 1 μg of DNA with the Fugene6 method (Boehringer Mannheim). After ~24 hours, selected culture cells were induced with TNF-α (10 ng/ml) or recombinant human IL-1β (10 ng/ml) or with phorbol 12-myristate 13-acetate (250 ng/ml) or ionomycin (10 ng/ml). All cell cultures were harvested 4 hours later, and luciferase activity was measured (Promega luciferase assay kit). Transfection control was measured with a renila luciferase vector with a thymidine kinase promoter or by protein concentration.
25. H. Zhong, H. SuYang, H. Erdjument-Bromage, P. Tempst, S. Ghosh, *Cell* **89**, 413 (1997).
26. S. C. Sun, J. Elwood, C. Beraud, W. C. Greene, *Mol. Cell. Biol.* **14**, 7377 (1994).
27. J. E. Thompson, R. J. Phillips, H. Erdjument-Bromage, P. Tempst, S. Ghosh, *Cell* **80**, 573 (1995).
28. R. Weil, C. Laurent-Winter, A. Israel, *J. Biol. Chem.* **272**, 9942 (1997).
29. F. Mercurio *et al.*, *Science* **278**, 860 (1997).
30. E. Zandi, D. M. Rothwarf, M. Delhase, M. Hayakawa, M. Karin, *Cell* **91**, 243 (1997).
31. Cells were harvested and blotted as previously described (*25*) with membranes probed with antibody to IκBα or IκBβ (C21 and C20; Santa Cruz Biotechnology, Santa Cruz, CA), polyclonal rabbit antibodies, or monoclonal mouse antibody to HA (12CA5). Immunoprecipitations were performed on transfected COS or 293 cells (3.5- and 10-cm plates, respectively), as previously described, with antibody to HA.
32. A. S. Raw, D. E. Coleman, A. G. Gilman, S. R. Sprang, *Biochemistry* **36**, 15660 (1997).
33. Single-letter abbreviations for the amino acid residues are as follows: A, Ala; C, Cys; D, Asp; E, Glu; F, Phe; G, Gly; H, His; I, Ile; K, Lys; L, Leu; M, Met; N, Asn; P, Pro; Q, Gln; R, Arg; S, Ser; T, Thr; V, Val; W, Trp; and Y, Tyr.

34. This work was supported by the Howard Hughes Medical Institute (HHMI) and NIH (S.G.) and by the National Creative Research Initiatives Program of the Korean Ministry of Science and Technology (J.W.L). C.F. was supported by Fonds Formation Chercheurs et Aide Recherche and HHMI, R.E.V. by Deutsche Forschungsgemeinschaft, and H.Z. by the Leukemia Society of America. We thank I. Douglas for technical help, P. J. Novick for the purified Sec4 protein, D. S. Na for helpful advice, and D. G. Schatz, D. Sengupta, H. J. Kim, and M. Solomon for careful reading of the manuscript.

14 October 1999; accepted 9 December 1999

Signaling and Circuitry of Multiple MAPK Pathways Revealed by a Matrix of Global Gene Expression Profiles

Christopher J. Roberts,[1]* Bryce Nelson,[2]* Matthew J. Marton,[1] Roland Stoughton,[1] Michael R. Meyer,[1] Holly A. Bennett,[1] Yudong D. He,[1] Hongyue Dai,[1] Wynn L. Walker,[1] Timothy R. Hughes,[1] Mike Tyers,[3] Charles Boone,[2]† Stephen H. Friend[1]†

Genome-wide transcript profiling was used to monitor signal transduction during yeast pheromone response. Genetic manipulations allowed analysis of changes in gene expression underlying pheromone signaling, cell cycle control, and polarized morphogenesis. A two-dimensional hierarchical clustered matrix, covering 383 of the most highly regulated genes, was constructed from 46 diverse experimental conditions. Diagnostic subsets of coexpressed genes reflected signaling activity, cross talk, and overlap of multiple mitogen-activated protein kinase (MAPK) pathways. Analysis of the profiles specified by two different MAPKs—Fus3p and Kss1p—revealed functional overlap of the filamentous growth and mating responses. Global transcript analysis reflects biological responses associated with the activation and perturbation of signal transduction pathways.

Mitogen-activated protein kinase (MAPK) cascades control changes in gene expression, cytoskeletal organization, and cell division (*1*). Genome-wide DNA microarrays are emerging as a powerful tool for broad correlation of gene activity with alterations in physiological or developmental states (*2–4*). Global expression profiles assembled from diverse ex-

periments have the potential to reveal the hierarchical connections between signal transduction pathways, the patterns of gene expression underlying complex biological responses, and the activity of specific pathways and effectors. To elucidate the signal circuitry and gene activity that specifies MAPK-regulated states, we used global transcript analysis to study activation and genetic perturbation of the budding yeast *Saccharomyces cerevisiae* pheromone response MAPK pathway.

During mating, haploid *MAT***a** and *MAT*α *S. cerevisiae* cells communicate with each other through secretion of peptide pheromones **a**- and α-factor, respectively, to which the opposite cell type responds. Pheromone stimulates yeast cells to increase the expression of mating genes, arrest cell division in the G_1 phase of the cell cycle, and form polarized mating projections directed toward the pheromone source (*5*). These responses are initiated by a cell surface receptor that couples to a heterotrimeric G protein and downstream MAPK kinase cascade (Fig. 1A). Three additional MAPK modules are potentially linked to the pheromone response pathway through functional relationships or shared components (Fig. 1A). The protein kinase C (PKC) pathway is activated by cell surface stress, which occurs during formation of the mating projection (*6*). The HOG pathway responds to hypertonic stress (*7*). The filamentous growth pathway responds to environmental and nutritional cues to promote haploid invasive growth on rich medium and diploid pseudohyphal development on medium low in nitrogen (*8*). Although components of the pheromone response pathway, such as Ste20p and Ste11p, form part of the HOG and filamentous growth MAPK pathways (*7*–*9*), their activation by high osmolarity or nutritional cues does not initiate a mating response in wild-type (wt) cells, which suggests that these signaling components assemble into functionally independent complexes (*7, 9*) (Fig. 1A). The pheromone and filamentous growth pathways both activate the transcription factor Ste12p (Fig. 1A). During pheromone signaling, Ste12p activates the promoters of mating genes either as a homomultimer bound to pheromone response elements (PREs) or as a heteromultimer with Mcm1p (*5*). During signaling of the filamentous growth pathway, Ste12p activates promoters that contain filamentation response elements as a heteromultimer with Tec1p (*8*).

To characterize the genome-wide changes in transcription that accompany pheromone signaling, DNA microarrays consisting of >97% of the known or predicted genes of *S. cerevisiae* were probed with differentially labeled (Cy3, green; Cy5, red) cDNA pools derived from pheromone-treated or mock-treated cells (*10, 11*). The relative abundance of each RNA message was measured by directly comparing the signals from competitive hybridizations, resulting in a red/green expression ratio for each gene. We first examined the pheromone-induced changes in gene expression (response profile) after exposure of *MAT***a** cells to α-factor concentrations ranging from 0.15 to 500 nM for 30 min. The response profile was relatively invariant above the 15.8 nM pheromone treatment, which suggests that the response was saturated; at 50 nM pheromone, expression of more than 200 genes was increased and expression of more than 200 genes was repressed (Fig. 2A) at a 99% confidence level (i.e., <1% chance the expression change was due to measurement errors alone) (*4, 11*). A genome-wide comparison of gene expression changes resulting from saturating treatments of 15.8 or 50 nM pheromone showed a strong correlation, which indicates that the results were highly reproducible (Fig. 2B) (ρ = 0.98) (*12*). We also examined the response of *MAT*α cells to **a**-factor. Unlike α-factor, **a**-

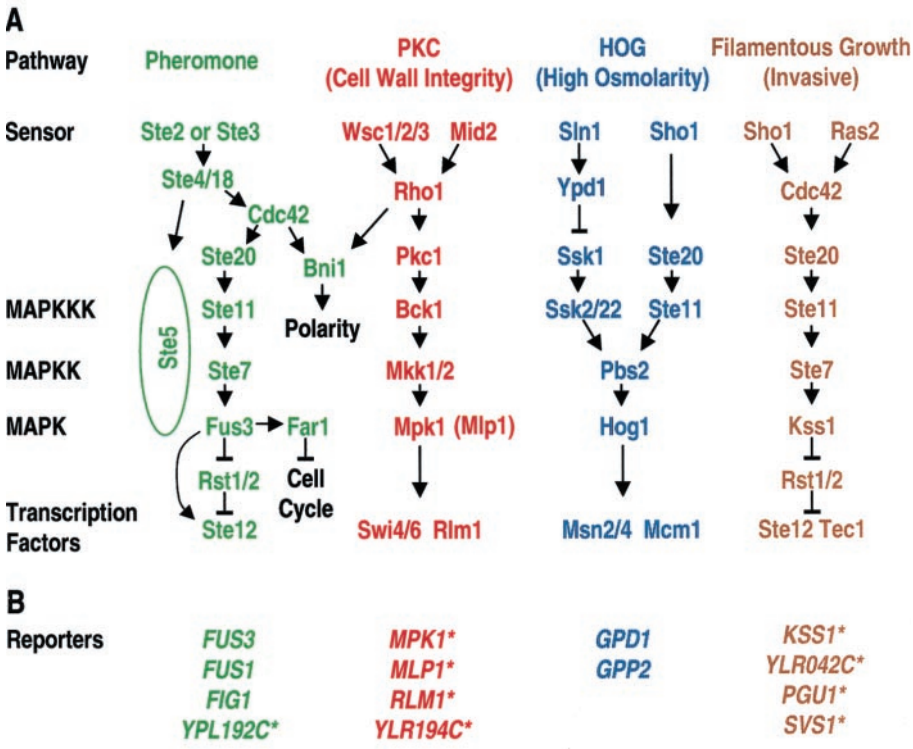

Fig. 1. Simplified schematic of four MAPK pathways in yeast. (**A**) During mating, peptide pheromones α-factor and **a**-factor activate the receptors Ste2p and Ste3p, respectively. Receptor stimulation releases free Gβγ (Ste4p/Ste18p) and leads to activation of the MAPK cascade. MAPK Fus3p activates both gene expression, by phosphorylation of the Ste12p transcription factor and its associated negative regulators Rst1p and Rst2p (*21*), and G_1 arrest, by phosphorylation of the cyclin-dependent kinase inhibitor Far1p (*19*). Cdc42p controls polarized morphogenesis through interactions with Bni1p and other polarity proteins linked to the actin cytoskeleton (*20, 24*). In the PKC pathway, signaling by Wsc1p/Wsc2p/Wsc3p and Mid2p (*30*) activates Rho1p, Pkc1p, and a MAPK module that culminates in Mpk1p (and probably Mlp1p), which control at least two transcription factors—Rlm1p and Swi4/Swi6p (*30*). Activated Rho1p also interacts with Bni1p (*20*). In the HOG pathway, hypertonic shock activates Sho1p and negatively regulates Sln1p, activating a MAPK module leading to Hog1p-dependent activation of transcription factors including Msn2/4p and Mcm1p (*31*). In the filamentous (diploid pseudohyphal and haploid invasive) growth pathway, Sho1p (*9*) and other sensors feed into two parallel pathways, one of which is a MAPK module that activates Kss1p, resulting in phosphorylation of Rst1p/Rst2p and activation of the Ste12p/Tec1p transcription factor complex (*8*). Not shown is a parallel branch of the filamentous growth pathway involving Ras2p/cAMP signaling (*32*). (**B**) Transcriptional reporter genes for activation of the MAPK pathways. *FUS1*, *FUS3*, and *FIG1* are known pheromone-induced mating genes (*14*); *GPD1* and *GPP2* encode proteins required for intracellular production of glycerol (*13*). Asterisks mark reporter genes identified in this study. *MPK1*, *MLP1*, *RLM1*, and *YLR194C* were induced under conditions that activate the PKC-regulated MAPK pathway; *KSS1*, *YLRO42C*, *PGU1*, and *SVS1* are potential filamentous growth genes induced preferentially by Kss1p signaling.

[1]Rosetta Inpharmatics, 12040 115th Avenue Northeast, Kirkland, WA 98034, USA. [2]Biology Department, Queen's University, Kingston, Ontario K7L 3N6, Canada. [3]Programme in Molecular Biology and Cancer, Samuel Lunenfeld Research Institute, Room 1080, Mount Sinai Hospital, 600 University Avenue, Toronto, Ontario M5G 1X5, Canada.

*These authors contributed equally to this work.
†To whom correspondence should be addressed. E-mail: boonec@biology.queensu.ca and sfriend@rii.com

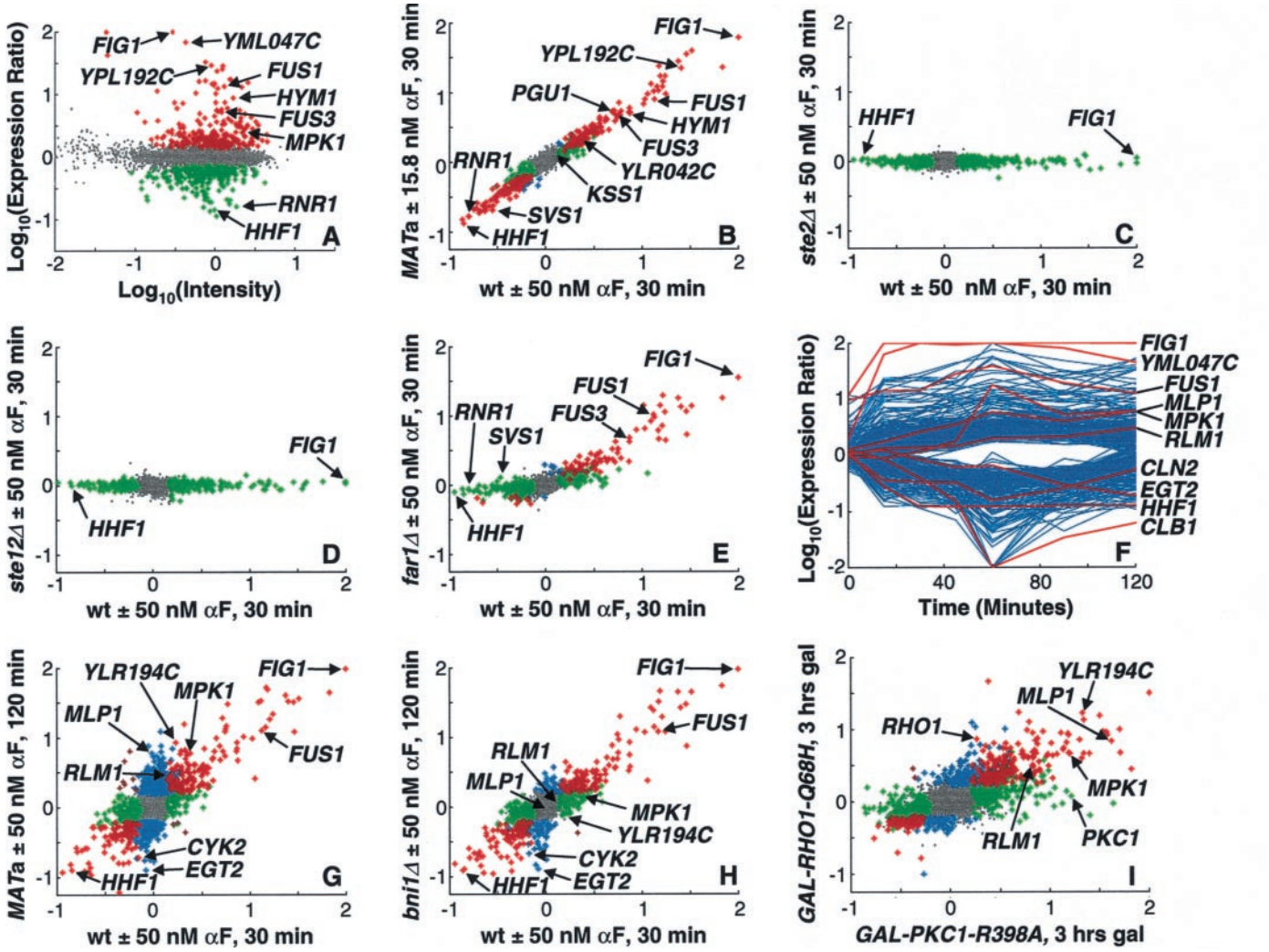

Fig. 2. DNA microarray analysis of *S. cerevisiae* pheromone response. (**A**) α-Factor response profile for the wt *MAT***a** strain R276 (*10, 28*). Fluorescently labeled cDNAs derived from wt cells either mock treated or treated with 50 nM α-factor for 30 min were hybridized competitively to four DNA microarrays, each containing >97% of all yeast open reading frames (*4*). Results from the four chips were averaged. Data are displayed as mean intensity [$\log_{10}$(intensity)] versus the red/green ratio [$\log_{10}$(expression ratio)] for each probe (*4*). Gray dots represent genes that showed no change in expression; genes that were induced or repressed by α-factor treatment, at a 99% confidence level (*4, 11*), are plotted as red stars (237 in total) or green stars (248 in total), respectively (*11, 14*). Genes labeled in the plots include previously identified (*FUS1*, *FIG1*) and novel (*YML047C*, *YPL192C*) pheromone-induced genes and mitotic cell cycle S phase–induced genes (*HHF1*, histone H4, and *RNR1*, ribonucleotide reductase large subunit). (**B**) Correlation plot of two different concentrations of α-factor (*4, 11*). Fluorescently labeled cDNAs derived from wt mock treated or treated with 15.8 nM α-factor for 30 min and wt mock treated or treated with 50 nM α-factor were analyzed on pairs of microarrays. Genes induced by the pheromone treatment are plotted as positive values. Log_{10} of the expression ratio for each gene derived from the 15.8 nM α-factor treatment is plotted versus $\log_{10}$ of the expression ratio in the 50 nM α-factor treatment. Genes whose expression did not change significantly in the two experiments are shown as gray dots; genes whose expression was induced or repressed, at a 99% confidence level, are plotted as colored stars. Red stars correspond to genes whose expression changed, either induced or repressed, in both experiments; green and blue stars correspond to genes whose expression changed only in a response profile plotted on the *x* and *y* axis, respectively. Spreadsheets listing the data for all genes shown as colored stars in the correlation plots within Figs. 2 and 3 are provided with the supplementary material (*11*). Response profile derived from the 30-min, 50 nM α-factor treatment of wt is plotted against the following competitive hybridizations. (**C**) R1269 (*ste2*Δ) mock treated versus treated with 50 nM α-factor for 30 min. (**D**) R418 (*ste12*Δ) mock treated versus treated with 50 nM α-factor for 30 min. (**E**) R496 (*far1*Δ) mock treated versus treated with 50 nM α-factor for 30 min. (**F**) Kinetic analysis of 50 nM α-factor treatment. Fluorescently labeled cDNAs derived from strain R276 (wt) mock treated versus treated with 50 nM α-factor for 0, 15, 30, 45, 60, 90, and 120 min. At each time point, samples of cells were examined microscopically to quantify the pheromone-induced changes in cell morphology (*18*). Genes whose expression ratio changed >2-fold in two or more experiments, for which data were obtained at a 99% confidence level in three or more experiments, are plotted (156 genes induced and 100 genes repressed). Most genes are plotted as blue lines and genes of interest are highlighted in red. (**G**) R276 (wt) mock treated versus treated with 50 nM α-factor for 120 min. Brown stars represent genes whose expression is anticorrelated (i.e., induced in one experiment but repressed in the other or vice versa). Several genes preferentially induced (*MPK1*, *MLP1*, *RLM1*, *YLR194C*) or repressed (*CYK2*, *EGT2*) at 120 min of pheromone treatment are labeled. (**H**) R994 (*bni1*Δ) mock treated versus treated with 50 nM α-factor for 120 min. (**I**) Expression profile derived from Y1469 (wt, carrying empty vector pRS316) versus Y1469 (carrying *GAL1/10pr-RHO1-Q68H*), both strains treated with 2% galactose for 3 hours, is plotted against the expression profile derived from Y1469 (carrying pRS316) versus Y1469 (carrying *GAL1/10pr-PKC1-R398A*), both strains treated with 2% galactose for 3 hours.

factor contains a COOH-terminal farnesyl modification and is secreted through a nonclassical pathway (*5*). Apart from mating-type–specific genes (e.g., *ASG7* in **a** cells and *MF*α*2* in α cells) (*13*), the **a**- and α-factor response profiles were highly correlated (*11*) (ρ = 0.92). Pheromone treatment caused increased expression of genes involved at each stage of the mating response (*5*). A large set of novel pheromone-induced genes was identified (*14*), and gene deletion experiments have demonstrated that some of these genes are required for efficient mating. For example, mutations that alter the highly conserved *HYM1* product cause defects in mating, pheromone-induced polarized morphogenesis, and basal expression of mating genes (*15*). Expression of genes that promote cell cycle progression, DNA replication, budding, and mitosis appeared to be repressed by pheromone treatment (*14*).

Analysis of *ste2*Δ cells, which carry a deletion of the gene encoding the α-factor receptor, revealed that the entire pheromone response profile was specified by the pheromone receptor (Fig. 2C). Several observations indicate that signaling, down to the level of Fus3p, takes place independently of Ste12p activation (*6, 16*). *ste4*Δ, *ste18*Δ, *ste5*Δ, *ste11*Δ, *ste7*Δ, *fus3*Δ *kss1*Δ, and *ste12*Δ mutant cells were all completely defective for pheromone-induced changes in transcription (Fig. 2D) (*17, 18*). Thus, the entire transcriptional response appears to be derived from pathway-dependent activation of Ste12p. This finding indicates that all functional links between upstream signaling molecules of the pheromone response pathway and other transcription factors must be regulated by a Ste12p-dependent circuit (*6*) and that disruption of signal transmission at intermediate steps does not result in cross-talk activation of other MAPK pathways (*9*).

To determine the effect of G_1 cell cycle arrest on pheromone-regulated gene expression, we examined cells lacking the cyclin-dependent kinase inhibitor Far1p. *far1*Δ cells have normal pheromone-dependent activation of Ste12p and increased transcription of *FUS1* but do not show G_1 cell cycle arrest (*19*). Comparison of the pheromone response profile of *far1*Δ cells with the response profile of wt cells showed that essentially all gene repression required Far1p (Fig. 2E). Thus, Ste12p controls repression through increased transcription of *FAR1*, whose activated product arrests cells at Start in late G_1 phase (*19*). Indeed, most of the pheromone-repressed genes we identified are subject to cell cycle regulation and are expressed preferentially outside G_1 phase (*14*).

After transcriptional activation and G_1 arrest, the pheromone signal initiates polarized cell growth to form a mating projection or "shmoo." These morphological changes result from localized cell surface expansion and depend on reorganization of the cortical actin cytoskeleton (*20*). To determine the changes in gene expression that correlate with projection formation, we exposed wt cells to 50 nM α-factor for up to 2 hours (Fig. 2F). Comparison of the response profile after 120 min with the profile after 30 min revealed a set of transcripts induced to a greater extent at 120 min (Fig. 2G). This set included transcripts from genes encoding MAPKs associated with the PKC pathway—*MPK1* and *MLP1* (*YKL161C*)—and a downstream transcriptional effector, *RLM1* (Fig. 1A), which suggests that transcription of these genes might be induced by PKC pathway signaling during polarized morphogenesis. To test this possibility, we examined *bni1*Δ mutant cells, which are defective in projection formation (*20*) and substantially delayed for pheromone-mediated activation of the PKC-regulated MAPK Mpk1p (*6*). Comparison of the pheromone response profile for *bni1*Δ cells at 120 min with wt cells at 30 min indicated that *bni1*Δ cells activated Ste12p and initiated G_1 arrest but did not show increased transcription of *MPK1* and other late-induced genes (Fig. 2H). Genes that showed increased transcription by extended pheromone treatments also showed increased transcription after overexpression of genes encoding constitutively active forms of Pkc1p and Rho1p from the inducible *GAL1/10* promoter (Fig. 2I). Moreover, many of these genes, including *MLP1* and *RLM1*, are pheromone-induced in an Mpk1p-dependent manner (*17*). Thus, temporal analysis of pheromone-dependent transcriptional changes identified genes induced by signaling of the PKC-regulated MAPK pathway during mating projection formation (*6*).

Two partially redundant negative regulators of Ste12p, called Rst1p (Dig1p) and Rst2p (Dig2p), prevent transcription of Ste12p target genes in the absence of signaling (*21*). Double-mutant cells, *rst1*Δ *rst2*Δ, that lack Rst1p Rst2p exhibit constitutive *FUS1* expression and invasive growth, which suggests that they express both mating and filamentation genes (Fig. 1A). The transcript profile of *rst1*Δ *rst2*Δ cells in the absence of pheromone (vegetative profile) showed abundant expression for mating genes without the concomitant repression of cell cycle genes (Fig. 3A). This profile is consistent with constitutive activation of Ste12p below the cell cycle control point at Fus3p (Fig. 1A). A gene set corresponding to potential filamentation genes was identified through their increased expression in the *rst1*Δ *rst2*Δ profile when compared with the pheromone response profile and includes *PGU1*, *YLR042c*, *SVS1*, and *KSS1* (Fig. 3A). *PGU1* and *YLR042c* also showed increased expression after pheromone treatment of wt cells (Fig. 2B), which suggests overlap between the mating and filamentation responses.

The MAPK that mediates activation of filamentous growth, Kss1p, should induce expression of bona fide filamentation genes regulated by Rst1p and Rst2p. In the absence of Fus3p, Kss1p is subject to activation by both basal and pheromone-induced signaling of the pheromone response pathway (*8*). To define gene sets induced specifically by Fus3p and Kss1p, we examined profiles derived from mutants defective for either MAPK. Both the vegetative and pheromone response profiles for *kss1*Δ cells were very similar to those of wt cells (*11*). Thus, global transcriptional changes directed by Fus3p resemble those observed for wt cells. The vegetative and pheromone response profiles for *fus3*Δ cells demonstrated that expression of *PGU1*, *YLR042c*, *SVS1*, *KSS1*, and other potential filamentation genes were induced preferentially by basal (Fig. 3B) or pheromone-induced Kss1p signaling (Fig. 3C) and that increased expression of these genes was Tec1p-dependent (Fig. 3D). The promoter sequences of *PGU1*, *YLR042c*, *SVS1*, and *KSS1* directed *lacZ* expression that was co-regulated with the Kss1p MAPK pathway-specific reporter *FG::Ty1-lacZ* (*11*). Thus, a set of filamentation genes defined from the *rst1*Δ *rst2*Δ profile appear to be under the control of Kss1p-activated Tec1p.

The S288c genetic background used in these experiments carries a *flo8* mutation that renders cells defective for both haploid invasive growth and diploid pseudohyphal development in response to environmental stimuli (*22*). However, *rst1*Δ *rst2*Δ mutant cells bypass the *FLO8* requirement and invade agar constitutively (*21*). This invasive phenotype may depend on increased transcription of the filamentation gene set, expression of the correlated pheromone-responsive gene set, or both. Apart from increased expression of the filamentation gene set, the pattern of constitutive gene expression of *rst1*Δ *rst2*Δ cells (Fig. 3A) resembles that of pheromone-stimulated *far1*Δ cells (Fig. 2E). To determine whether the filamentation genes are responsible for the haploid invasive growth of *rst1*Δ *rst2*Δ cells, we examined whether pheromone could stimulate this process. Surprisingly, pheromone signaling caused cell adhesion and agar invasion of *far1*Δ cells (Fig. 4). Similarly, for wt cells, agar invasion was stimulated by nonsaturating pheromone doses that were below the threshold for G_1 arrest (Fig. 4). Pheromone-induced invasion was also observed for *kss1*Δ and *tec1*Δ mutants but not for pheromone response pathway mutants such as *ste12*Δ and *ste2*Δ cells (Fig. 4) (*23*). Thus, it appears that partial activation of pheromone-responsive genes in the absence of G_1 cell cycle arrest initiates a developmental program that resembles haploid invasive

growth. Because pheromone response is sensitive to gradients (*24*) and low levels of pheromone cause cells to switch from an axial to a bipolar budding pattern (*25*), pheromone-induced invasion may enable elongation and growth of dividing cells toward a diffuse pheromone source and thereby facilitate mating among haploid cells within dispersed populations.

We performed two-dimensional hierarchical clustering analysis of 46 experiment profiles and 383 genes (represented by 400 microarray probes), whose expression changed more than threefold, at a 99% confidence level, in at least two different experiments. This method identified sets of experiments that lead to similar global patterns of gene expression and sets of genes subject to similar regulation. In the resultant two-dimensional plot (Fig. 5A), the gene cluster tree is represented on the horizontal axis and the experimental cluster tree is on the vertical axis. Patches of red (gene induction) and green (gene repression) identify gene sets that show co-regulation across multiple correlated experiments.

Experimental profiles 1 to 31 encompass conditions that activate the pheromone response pathway. Most of these experiments showed increased expression of a pheromone-induced gene set (genes 150 to 265) and decreased expression of a cell cycle–regulated gene set (genes 1 to 121). However, experiments 20 to 22, which include the vegetative profile (unstimulated) of *rst1*Δ *rst2*Δ cells and the pheromone response profile of *far1*Δ cells, showed increased expression of pheromone-induced genes with little or no gene repression. Experiments 26 to 31, which include the response associated with nonsaturating pheromone doses, short pheromone treatments, and mutants compromised for signaling (*fus3*Δ, *fus3-K42R*, *ste20*Δ, *rst1*Δ *rst2*Δ), showed increased expression of a subset of pheromone-responsive genes. Experiments 36 and 37 correspond to the overexpression of dominant-activated alleles of *PKC1* and *RHO1* and define a candidate cluster of PKC-regulated genes (genes 289 to 378). Experiments 38 to 44 include the vegetative profiles of pheromone response pathway signaling mutants and identify genes regulated by basal signaling of the pathway (*26*).

Expanded views of selected gene clusters are shown in Fig. 5B. The genes in cluster I were repressed by brief pheromone treatments and include several genes activated early in the cell cycle during the G_1-to-S transition (*3*). In general, the genes in cluster II were repressed by longer pheromone treatments and activated late in the cell cycle during the M-to-G_1 transition. Genes in clusters III and V were induced by brief pheromone treatments and *STE12* overexpression but were repressed in pheromone response pathway mutants. The pheromone-responsive genes in cluster VII displayed a more complex pattern of regulation and appear to be activated by Ste12p indirectly through PKC pathway signaling. These genes were induced by extended pheromone treatments (60 to 120 min) and overexpression of the dominant-activated alleles of *PKC1* and *RHO1*, but they were not induced in response to *STE12* overexpression or pheromone treatment of *bni1*Δ cells. Consistent with these observations, clusters III and V, but not VII, were enriched for potential Ste12p binding PREs (*11*). Several different clusters contain genes that appear to be regulated by Kss1p signaling (Fig. 3, B and C). Cluster IV contains *PGU1*, cluster VI contains *YLR042c*, and cluster VIII contains *KSS1*. Indeed, promoter analysis revealed that the genes within these clusters were enriched for Tec1p binding sites (*11*). The absence of coherent clustering by these genes indicates that each set is subject to additional, unique modes of regulation; however, co-regulation of these genes was observed in seven experiments (Fig. 5B, black arrowheads) (*27*). Several of the Kss1p-regulated genes may participate in cell surface remodeling during filamentous growth (*27*).

Genome-wide transcript analysis simultaneously monitors the gene expression programs of all signal transduction pathways. In addition to identifying the gene sets regulated by particular pathways, internal feedback regulatory loops also may be uncovered. For

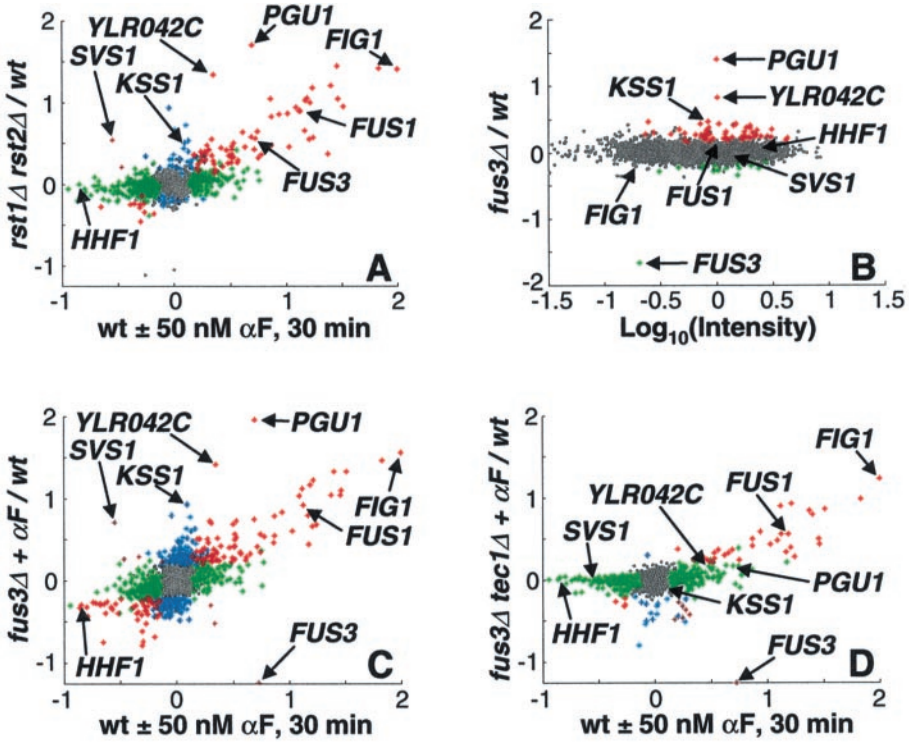

Fig. 3. Derepression of mating and filamentation genes in cells defective for Ste12p regulation. Correlation plots of expression profiles for two different microarray experiments are shown in (A), (C), and (D); in each case, the response profile derived from the 50 nM α-factor treatment of wt strain R276 is plotted on the *x* axis. Data representation is described in Fig. 2 legend. (**A**) Vegetative profile of R4063 (*rst1*Δ *rst2*Δ) cells; genes induced in the *rst1*Δ *rst2*Δ cells relative to wt cells are plotted as positive values. (**B**) Vegetative profile of R500 (*fus3*Δ) cells; changes in gene expression are plotted against the mean intensity of each spot (genes labeled as in Fig. 2A). (**C**) R426 (wt) cells mock treated versus R500 (*fus3*Δ) treated with 50 nM α-factor for 30 min. (**D**) R426 (wt) cells mock treated versus Y1787 (*fus3*Δ *tec1*Δ) treated with 50 nM α-factor for 30 min.

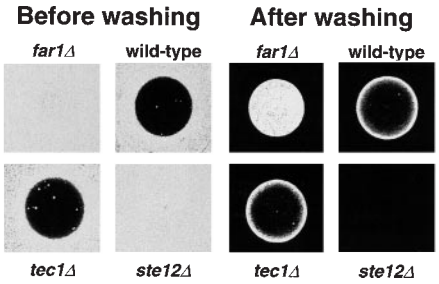

Fig. 4. Pheromone-induced agar invasion. One microliter of α-factor (1 mM) was applied to a lawn of *MAT***a** *bar1*Δ cells (R426, wt; R418, *ste12*Δ; R496, *far1*Δ; Y1543, *tec1*Δ) (*28*) spread on the surface of agar plates containing rich medium. Before washing, plates were incubated for 2 days and then imaged to record the extent of pheromone-induced growth inhibition. After washing under running tap water, the plates were imaged to record the cells that adhered to one another and invaded into the agar substrate.

example, expression of genes encoding four of the six yeast MAPKs (Fus3p, Kss1p, Mpk1p, and Mlp1p) is increased by stimulation of their cognate pathways (Fig. 1B). Global profiling also reveals higher order signaling circuits, such as sequential activation of the yeast pheromone response and PKC-regulated MAPK pathways during mating projection formation. Genome-wide tran-

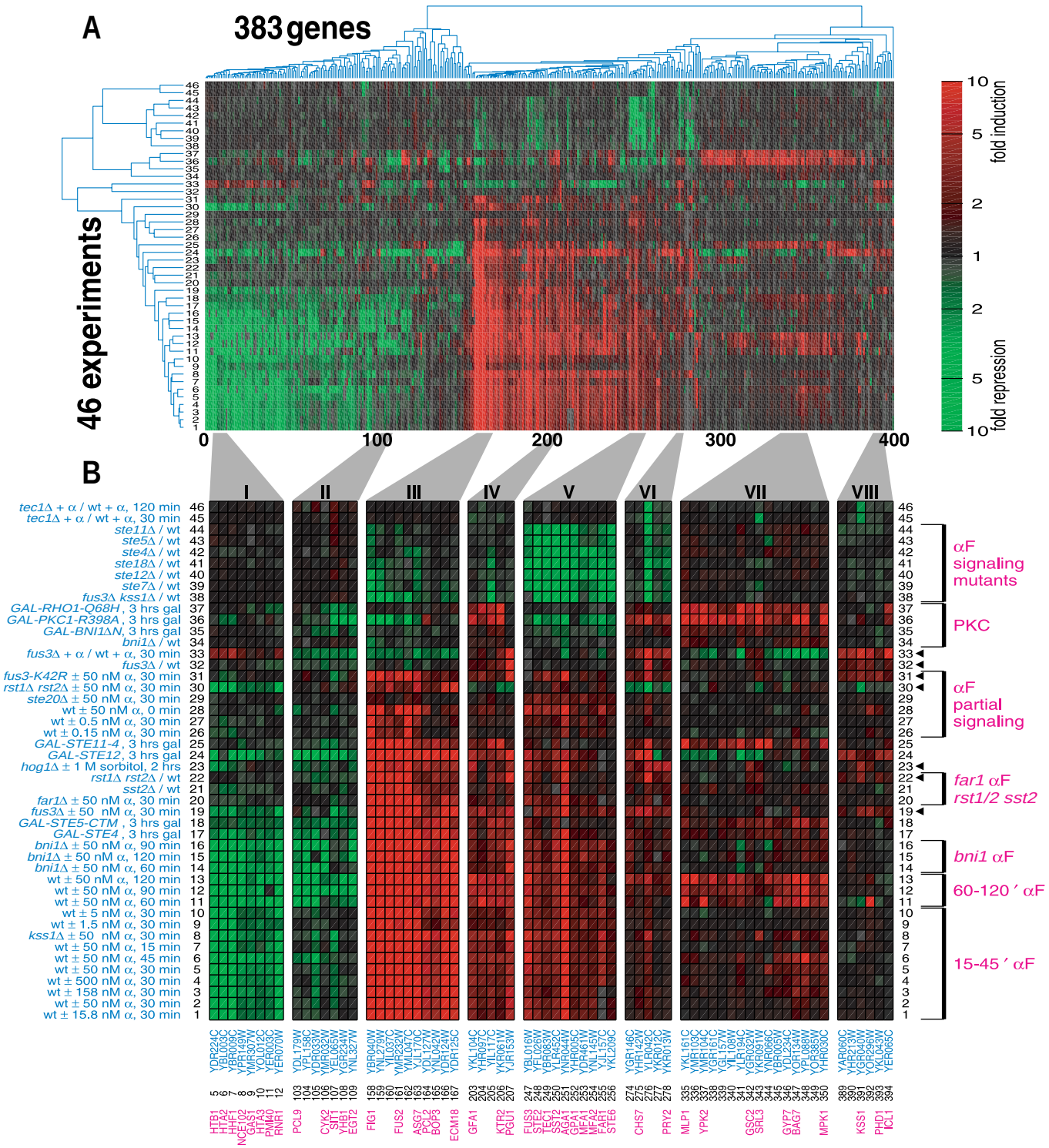

Fig. 5. Two-dimensional clustering analysis of experimental expression profiles and gene behavior. (**A**) Three hundred eighty-three genes whose expression was induced or repressed greater than threefold, at a 99% confidence level, in any two microarray experiments, were clustered by the correlation of their response signatures (*33*). Forty-six experiments were clustered by the correlation of their signatures. Genes are plotted along the horizontal axis, with the gene cluster tree above. Experiments are plotted along the *y* axis, with the experiment cluster tree on the outer leftmost side of the plot. Increases in mRNA levels are represented as shades of red, and decreases in mRNA levels are represented as shades of green. (**B**) Sections of (A) are expanded to allow visualization of specific gene clusters (labeled I to VIII). Experiment names are listed on the left and gene names are at the bottom. Experiment clusters are labeled on the right. Seven experiments that show changes in expression of Kss1p-regulated genes are labeled with arrowheads on the right (*27*).

scriptional profiling thus provides a means to trace the signaling mechanisms and circuits that underlie complex biological responses.

References and Notes

1. I. Herskowitz, *Cell* **80**, 187 (1995); D. E. Levin and B. Errede, *Curr. Opin. Cell Biol.* **7**, 197 (1995); H. D. Madhani and G. R. Fink, *Trends Genet.* **14**, 151 (1998); H. J. Schaeffer and M. J. Weber, *Mol. Cell. Biol.* **19**, 2435 (1999).
2. J. DeRisi *et al.*, *Nature Genet.* **14**, 457 (1996); J. L. DeRisi, V. R. Iyer, P. O. Brown, *Science* **278**, 680 (1997); D. A. Lashkari *et al.*, *Proc. Natl. Acad. Sci. U.S.A.* **94**, 13057 (1997); L. Wodicka *et al.*, *Nature Biotechnol.* **15**, 1359 (1997); F. C. Holstege *et al.*, *Cell* **95**, 717 (1998); M. B. Eisen, P. T. Spellman, P. O. Brown, D. Botstein, *Proc. Natl. Acad. Sci. U.S.A.* **95**, 14863 (1998); S. Chu *et al.*, *Science* **282**, 699 (1998); D. Fambrough, K. McClure, A. Kazlauskas, E. S. Lander, *Cell* **97**, 727 (1999); V. R. Iyer *et al.*, *Science* **283**, 83 (1999).
3. P. T. Spellman *et al.*, *Mol. Biol. Cell* **9**, 3273 (1998); R. J. Cho *et al.*, *Mol. Cell* **2**, 65 (1998).
4. M. J. Marton *et al.*, *Nature Med.* **4**, 1293 (1998).
5. G. F. Sprague Jr. and J. W. Thorner, in *The Molecular and Cellular Biology of the Yeast* Saccharomyces cerevisiae, vol. 2, *Gene Expression* (Cold Spring Harbor Laboratory Press, Cold Spring Harbor, NY, 1992), p. 657; E. Leberer, D. Y. Thomas, M. Whiteway, *Curr. Opin. Genet. Dev.* **7**, 59 (1997).
6. P. Zarzov, C. Mazzoni, C. Mann, *EMBO J.* **15**, 83 (1996); B. M. Buehrer and B. Errede, *Mol. Cell. Biol.* **17**, 6517 (1997).
7. F. Posas and H. Saito, *Science* **276**, 1702 (1997).
8. H. D. Madhani and G. R. Fink, *Science* **275**, 1314 (1997); H. D. Madhani, C. A. Styles, G. R. Fink, *Cell* **91**, 673 (1997); R. L. Roberts and G. R. Fink, *Proc. Natl. Acad. Sci. U.S.A.* **95**, 13783 (1998); H.-U. Mosch *et al.*, *Mol. Biol. Cell* **10**, 1325 (1999).
9. S. M. O'Rourke and I. Herskowitz, *Genes Dev.* **12**, 2874 (1998).
10. For the α-factor experiments, overnight yeast cultures were grown for three generations to midlogarithmic phase (1×10^7 cells per milliliter) in rich medium (YPD) before they were split, and synthetic α-factor (Sigma-Aldrich) or water (for mock treatment) was added. Similar experiments involved treatments with synthetic **a**-factor in methanol [C. B. Xue, G. A. Caldwell, J. M. Becker, F. Naider, *Biochem. Biophys. Res. Commun.* **162**, 253 (1989)]; for the mock treatment, an equal volume of methanol was added. For the *fus3-K42R* experiment (Fig. 5, experiment 31), R500 (*fus3*Δ) (*28*) cells carrying the plasmid pJB290 (*29*) were grown to midlogarithmic phase in synthetic complete (SC) medium lacking leucine and then resuspended in an equal volume of YPD for 90 min before addition of α-factor. For experiments in the absence of α-factor, cells were grown to midlogarithmic phase in SC medium before harvesting. For galactose induction experiments, wt Y1469 cells harboring different plasmids were grown to midlogarithmic phase in SC medium containing 2% raffinose and lacking the appropriate nutrients for plasmid selection. Galactose was added to a final concentration of 2% (3-hour treatment). For sorbitol induction experiments, R7326 (*hog1*Δ) cells were grown in YPD to midlogarithmic phase before an equal volume of either YPD or YPD containing 2 M sorbitol was added (2-hour treatment). RNA from the α-factor kinetics and titration experiments (Fig. 5, experiments 1 to 7, 9 to 13, and 26 to 28) was isolated as described (*4*). All other experiments involved pelleting cells and freezing them in liquid nitrogen. Cells were then incubated in hot phenol: chloroform (50:50, v/v) and breakage buffer (*4*) for 5 min before vortexing (20 s). After the phases were separated, the aqueous phase was reextracted and vortexed (10 s) with phenol:chloroform (50:50, v/v). The RNA was concentrated with a microconcentrator (Amicon, Beverly, MA). Isolation of polyadenylated RNA and production of fluorescently labeled cDNAs were done as described (*4*). For each experiment described in this study, the data presented represent averaged results from hybridization to at least two DNA microarrays with fluor reversal (*4*).
11. The following supplementary materials can be found at the accompanying Web sites (www.rii.com and www.sciencemag.org/feature/data/1043534.shl): a description of the error model used to assign confidence levels to microarray measurements; data plots for additional experiments; spreadsheets containing data for all microarray experiments (including signal intensities, mean expression ratios, and *P* values for all genes); spreadsheets for the correlation plots in Figs. 2 and 3, which identify genes corresponding to colored stars; *lacZ* reporter analysis for promoters of pheromone- and Kss1p-regulated genes; and promoter analysis of the gene clusters in Fig. 5B.
12. Correlation plots (Fig. 2, B to E and G to I; Fig. 3, A, C, and D) display the expression ratio for each gene in one experiment versus the expression ratio in another experiment. The degree of correlation between experiments is quantified by calculating the correlation coefficient ρ for the union of genes induced or repressed at a given confidence level in either experiment (*4*). For this study, ρ was calculated at a 99% confidence level; therefore, the expression ratio for a given gene was considered statistically significant if the gene had a $<1\%$ chance of having an expression ratio departing from unity due to measurement errors alone. Coefficients for the correlation plots shown are given for genes that were significantly reduced or repressed in one or both experiments (sig) and for all genes (all): Fig. 2B, $\rho = 0.98$ (sig), 0.92 (all); Fig. 2C, $\rho = -0.05$ (sig), 0.0 (all); Fig. 2D, $\rho = 0.01$ (sig), 0.02 (all); Fig. 2E, $\rho = 0.79$ (sig), 0.68 (all); Fig. 2G, $\rho = 0.69$ (sig), 0.60 (all); Fig. 2H, $\rho = 0.87$ (sig), 0.78 (all); Fig. 2I, $\rho = 0.76$ (sig), 0.65 (all); Fig. 3A, $\rho = 0.66$ (sig), 0.54 (all); Fig. 3C, $\rho = 0.66$ (sig), 0.56 (all); Fig. 3D, $\rho = 0.61$ (sig), 0.40 (all).
13. To conserve space, we have referenced literature for yeast genes selectively. References for all the genes mentioned in this study can be found at The Proteome (http://www.proteome.com/) and the *Saccharomyces* Genome Database (http://genome-www.stanford.edu/Saccharomyces/).
14. A number of pheromone-induced genes have been identified in previous studies (*5*) [S. Erdman, L. Lin, M. Malczynski, M. Snyder, *J. Cell Biol.* **140**, 461 (1998)]. Of the 14 genes induced more than 10-fold in Fig. 2A (wt cells exposed to 50 nM α-factor for 30 min), 6 were previously uncharacterized: *YML047C*, *YLR445W*, *YIL037C*, *YPL192C*, *YNL279W*, and *YDR124W* (excluding genes whose promoters contain Ty elements, which are induced by pheromone treatment). Of the 55 genes induced threefold or more, 27 have no known cellular function (*11*, *13*). Of the 247 pheromone-repressed genes in Fig. 2A, 187 were previously identified as cell cycle regulated by DNA microarray experiments (*3*). Because the remaining 60 genes are subject to *FAR1*-dependent repression, they also may be cell cycle regulated.
15. M. Karos and R. Fischer, *Mol. Gen. Genet.* **260**, 510 (1999); P. Nair, B. Nelson, C. Roberts, C. Boone, unpublished observations.
16. A. Gartner, K. Nasmyth, G. Ammerer, *Genes Dev.* **6**, 1280 (1992); E. A. Elion, B. Satterberg, J. E. Kranz, *Mol. Biol. Cell* **4**, 495 (1993); Z. Zhou *et al.*, *Mol. Cell. Biol.* **13**, 2069 (1993); L. J. W. M. Oehlen, J. D. McKinney, F. R. Cross, *Mol. Cell. Biol.* **16**, 2830 (1996).
17. S. Ashkar *et al.*, data not shown.
18. As a control for the reduced level of *STE2* expression that occurs in signaling mutants [J. J. Hwang-Shum, D. C. Hagen, E. E. Jarvis, C. A. Westby, G. F. Sprague Jr., *Mol. Gen. Genet.* **227**, 197 (1991)] (*26*) (Fig. 5, experiments 38 to 44), we analyzed *ste12*Δ cells that expressed *STE2* from the constitutive *ADH1* promoter. We also analyzed *ste12*Δ cells after a 2-hour pheromone treatment. In both cases, we failed to detect any pheromone-induced changes in mRNA levels. The expression profiles for *ste4*Δ, *ste18*Δ, *ste5*Δ, *ste11*Δ, *ste7*Δ, and *fus3*Δ *kss1*Δ strains treated with α-factor were essentially identical to those for *ste2*Δ and *ste12*Δ (*17*). For each point in the time course of α-factor treatment shown in Fig. 2F, >300 cells were examined microscopically and classified as budded, unbudded, and with or without mating projections (shmoos). The percentage of cells in G_1 was calculated as the sum of the unbudded cells plus shmoos divided by the total. The percentages of budded cells, unbudded cells, shmoos, and G_1 cells for each time point were as follows: 52.9, 47.1, 0, and 47.1 for 0 min; 55.9, 36.8, 7.3, and 44.1 for 15 min; 47.1, 32, 20.9, and 52.9 for 30 min; 33.1, 39.8, 27.1, and 66.9 for 45 min; 3.7, 27.1, 69.1, and 96.2 for 60 min; 0.3, 8.6, 91.1, and 99.7 for 90 min; and 0, 1.6, 98.4, and 100 for 120 min. For the 120-min α-factor treatments, the percentages of shmoos were 98.4 and 32.7 for wt (Fig. 2G) and *bni1*Δ (Fig. 2H) cells, respectively.
19. F. Chang and I. Herskowitz, *Cell* **63**, 999 (1990); M. Peter *et al.*, *Cell* **73**, 747 (1993).
20. M. Evangelista *et al.*, *Science* **276**, 118 (1997); G. C. Chen, Y. J. Kim, C. S. Chan, *Genes Dev.* **11**, 2958 (1997); J. L. Brown *et al.*, *Genes Dev.* **11**, 2972 (1997); T. Fujiwara *et al.*, *Mol. Biol. Cell* **9**, 1221 (1998).
21. K. Tedford *et al.*, *Curr. Biol.* **7,** 228 (1997); J. G. Cook, L. Bardwell, S. J. Kron, J. Thorner, *Genes Dev.* **10**, 2831 (1996); L. Bardwell *et al.*, *Proc. Natl. Acad. Sci. U.S.A.* **95**, 15400 (1998).
22. H. Liu, C. A. Styles, G. R. Fink, *Genetics* **144**, 967 (1996).
23. *FLO11* expression plays an important role in the invasion stimulated by the filamentous pathway [W.-S. Lo and A. Dranginis, *Mol. Biol. Cell* **9**, 161 (1998); S. Rupp *et al.*, *EMBO J.* **16**, 1257 (1999)]. Changes in *FLO11* transcript levels were not detected in any experiments, likely because our experiments involved S288c (*flo8*) cells. We observed that α-factor induced invasion of *MAT***a** cells derived from the Σ1278b background, which contains wt alleles of *FLO8* and *FLO11*. Σ1278b *MAT***a** *flo11*Δ cells were also competent for pheromone-induced invasion (*17*), confirming that this process does not require *FLO11*. Pheromone-induced invasion occurs on both rich and synthetic complete medium, which suggests that this process does not involve a nutritional input.
24. A. Nern and R. A. Arkowitz, *Nature* **391**, 195 (1998); A. C. Butty *et al.*, *Science* **282**, 1511 (1998).
25. R. Dorer, P. M. Pryciak, L. H. Hartwell, *J. Cell Biol.* **131**, 845 (1995); S. Erdman and M. Snyder, personal communication.
26. S. Fields, D. T. Chaleff, G. F. Sprague Jr., *Mol. Cell. Biol.* **8**, 551 (1988); M. Whiteway *et al.*, *Cell* **56**, 467 (1989); D. C. Hagen, G. McCaffrey, G. F. Sprague Jr., *Mol. Cell. Biol.* **11**, 2952 (1991).
27. Potential filamentation genes were induced in experiments 19, 22, 23, 31, 32, and 33, which includes the pheromone response profile of *fus3*Δ cells, the *rst1*Δ *rst2*Δ profile, and the high osmolarity cross talk of *hog1*Δ cells (*9*), and coordinately repressed in experiment 30, the pheromone response profile of *rst1*Δ *rst2*Δ cells. Genes encoding secreted proteins (*PGU1* and *PRY2*), potential cell-surface proteins (*YLR042c*, *YIL117c*), proteins involved in glycosylation and chitin biosynthesis (*KTR2*, *CHS7*, and *GFA1*), and a regulatory protein implicated in invasive and filamentous growth (*PHD1*) were all induced by Kss1p signaling. *PGU1* encodes a secreted form of a pectin-degrading enzyme, which might facilitate yeast invasion of fruits [P. Blanco, C. Sieiro, N. M. Reboredo, T. G. Villa, *FEMS Microbiol. Lett.* **164**, 249 (1998); S. Gognies, A. Gainvors, M. Aigle, A. Belarbi, *Yeast* **15**, 11 (1999)]. Consistent with our results, *PGU1* has recently been shown to be induced by Kss1p signaling in Σ1278b cells [H. D. Madhani, T. Galitski, E. S. Lander, G. R. Fink, *Proc. Natl. Acad. Sci. U.S.A.* **96**, 12530 (1999)]. It is also noteworthy that α-factor treatment of *rst1*Δ *rst2*Δ cells leads to further induction of several pheromone-responsive genes (*11*). Pheromone-induced gene expression in the absence of Rst1p and Rst2p indicates that Ste12p activation may be controlled by another negative regulatory mechanism, perhaps one involving Kss1p [J. G. Cook, L. Bardwell, J. Thorner, *Nature* **390**, 85 (1997); L. Bardwell *et al.*, *Genes Dev.* **12**, 2887 (1998)]. Alternatively, Fus3p may phosphorylate and activate Ste12p directly [W. Hung, K. A. Olson, A. Breitkreutz, I. Sadowski, *Eur. J. Biochem.* **245**, 241 (1997)].
28. All yeast strains were based on the S288c genetic background and were derived from BY4741 (*MAT***a** *ura3*Δ*0 leu2*Δ*0 his3*Δ*1 met15*Δ*0*) or BY4742 (*MAT*α *ura3*Δ*0 leu2*Δ*0 his3*Δ*1 lys2*Δ*0*) [C. B. Brachmann *et*

al., *Yeast* **14**, 115 (1998)]. The *bar1*Δ (R276) and *hog1*Δ (R7326) deletions were constructed by gene replacement in BY4741 with the KanMX cassette [A. Wach, A. Brachat, R. Pohlmann, P. Philippsen, *Yeast* **10**, 1793 (1994)]. R426, the control strain for mutant experiments, was created by integration of *URA3* at the *ura3Δ0* locus in R276. Genes were deleted from derivatives of R276 and replaced with *URA3* sequences [J. S. Jones and L. Prakash, *Yeast* **6**, 363 (1990)], creating the following strains: *ste2*Δ (R1269), *ste4*Δ (R410), *ste5*Δ (R413), *ste7*Δ (R415), *ste11*Δ (R416), *ste12*Δ (R418), *ste18*Δ (R419), *ste20*Δ (R421), *fus3*Δ (R500), *kss1*Δ (Y1399), *bni1*Δ (R994), *sst2*Δ (R1331), *far1*Δ (R496), and *tec1*Δ (Y1543). Y1787 (*fus3*Δ *tec1*Δ) was created by replacing the *FUS3* gene of Y1543 with *LEU2* sequences. Y1460 (*MAT***a** *fus3*Δ *kss1*Δ *lys2Δ0*) was isolated by sporulation of the diploid formed by crossing R500 and Y1438 (*MAT*α *kss1Δ::URA3 bar1Δ::KanMX his3Δ200 leu2Δ0 met15Δ0 lys2Δ0*). Y1612 (*MAT***a** *rst1*Δ *rst2*Δ *lys2Δ0*) was isolated by sporulation of a diploid formed by crossing Y1458 (*MAT***a** *rst1Δ::URA3 rst2Δ::KanMX his3Δ200 leu2Δ0 lys2Δ0*) and Y1400 (*MAT*α *rst1Δ::URA3 bar1Δ::KanMX his3Δ200*). Y1469 (*MAT***a** *bar1Δ::KanMX trp1-63 his3Δ200 leu2Δ0 ura3Δ0 met15Δ0*) was isolated from sporulation of the diploid formed by crossing R276 and R154 (*MAT*α *lys2Δ0 ura3Δ0 trp1-63*).

29. Plasmids described previously include the following: pRS314 (CEN *TRP1*), pRS315 (CEN *LEU2*), and pRS316 (CEN *URA3*) [R. S. Sikorski and P. Hieter, *Genetics* **122**, 19 (1989)]; YCplac111 (CEN *LEU2*) and YCplac22 (CEN *TRP1*) [R. D. Gietz and A. Sugino, *Gene* **74**, 527 (1988)]; pDL242 carries the *GAL1/10* promoter (pr) regulating *PKC1-R398A* [M. Watanabe, C. Y. Chen, D. E. Levin, *J. Biol. Chem.* **269**, 16829 (1994)]; pL914 carries *GAL1/10pr-RHO1-Q68H* [H. Qadota *et al.*, *Science* **272**, 279 (1996)]; p2107 carries *GAL1/10pr-STE4* in vector pRS315; pGFP-GS5-CTM carries the *GAL1/10pr-GFP-STE5-CTM* [P. M. Pryciak and F. A. Huntress, *Genes Dev.* **12**, 2684 (1998)]; p2087, CEN *TRP1* plasmid, carries *GAL1/10pr-STE11-4*; pNC252, CEN *URA3* plasmid, carries *GAL1/10pr-STE12*. p356 carries *GAL1/10pr-BNI1ΔN* (*20*) in vector pRS316; pJB290 (CEN *LEU2*) carries a *FUS3* kinase dead allele, *fus3-K42R* (*8*); and p3019 (CEN *LEU2*) carries *FG::TY1-lacZ* (*8*). V85, a YCplac111-based plasmid containing the *lacZ* gene, was used for reporter construction. Promoter sequences were amplified by polymerase chain reaction (PCR) from W303-1A (*MAT***a** *ura3-1 leu2-3,112 his3-11,15 trp1-1 ade2-1 can1-100*) genomic DNA. The 3′ downstream primer included the start codon of the gene designed for an in-frame fusion with *lacZ*. The 5′ upstream primer determined the size of the promoter-containing PCR product: *YLR042C*, 600 base pairs (bp); *PGU1*, 743 bp; *FUS3*, 690 bp; *KSS1*, 791 bp; *FUS1*, 834 bp; *FIG1*, 800 bp; *SVS1*, 793 bp; *YPL192C*, 800 bp.
30. J. V. Gray *et al.*, *EMBO J.* **16**, 4924 (1997); J. Verna *et al.*, *Proc. Natl. Acad. Sci. U.S.A.* **94**, 13804 (1997); T. Ketela, R. Green, H. Bussey, *J. Bacteriol.* **181**, 3330 (1999); M. Rajavel *et al.*, *Mol. Cell. Biol.* **19**, 3969 (1999); K. S. Lee *et al.*, *Mol. Cell. Biol.* **13**, 3067 (1993); Y. Watanabe, K. Irie, K. Matsumoto, *Mol. Cell. Biol.* **15**, 5740 (1995); Y. Watanabe *et al.*, *Mol. Cell. Biol.* **17**, 2615 (1997); K. Madden *et al.*, *Science* **275**, 1781 (1997).
31. M. H. Kuo, E. T. Nadeau, E. J. Grayhack, *Mol. Cell. Biol.* **17**, 819 (1997); W. Gorner *et al.*, *Genes Dev.* **12**, 586 (1998).
32. M. C. Lorenz and J. Heitman, *EMBO J.* **17**, 1236 (1998).
33. Hierarchical clustering analysis [see, e.g., J. A. Hartigan, *Clustering Algorithms* (Wiley, New York, 1975)] was performed in both the experiment and gene dimensions. The distance metric was defined as $D = 1 - \rho$, where ρ is the correlation coefficient between the expression changes seen in any two genes across all experiments in the set or, alternatively, between any two experiment profiles across all genes. These expression changes were quantified as $\log_{10}$(expression ratio) where the ratio is between the treated and untreated condition. The color display encodes $\log_{10}$(expression ratio) as color, where red is up-regulation, green is down-regulation, and black represents no change, as illustrated in the color bar of Fig. 5A (gray denotes no reliable data). Each row in the display represents an experiment condition pair, and each column corresponds to a gene. Rows and columns are displayed in the order given by the clustering output trees in the two dimensions. The clustering operation and this rearrangement are independent and noninterfering between the two dimensions. Not all genes are retained in the clustering analysis, only those that had a minimum amplitude of response of threefold at a 99% confidence level (*4, 11*) in at least two experiments. This focuses attention on the most informative genes, but it does not bias the clustering result toward any a priori assumptions about the mechanism. The growth conditions, strains, and plasmids for the experiments included in Fig. 5 were as described in (*10, 28, 29*). The 46 experiments whose response profiles were clustered in Fig. 5 include those described in Figs. 2 and 3 as well as the experiments described below. Experiments 1 to 5, 9, 10, 26, and 27 involved various concentrations of α-factor, each for a 30-min treatment of R276 (wt) cells. Experiments 2, 5, 6, 7, 11 to 13, and 28 correspond to a kinetic analysis of α-factor response for R276 (wt) cells (Fig. 2F). Experiments 2 and 5 involved identical α-factor treatments for R276 (wt) cells, which provided the data for the "wt ± 50 nM αF, 30 min" experiment shown in the correlation plots of Figs. 2 and 3. Experiments 14, 15, and 16 (Fig. 2H) correspond to the α-factor response of *bni1*Δ cells. Experiments 17, 18, 24, 25, and 35 to 37 involved galactose induction of *STE4*, *STE5-CTM* (*GFP-STE5-CTM*), *STE12*, *STE11-4*, *BNI1ΔN*, *PKC1-R398A*, and *RHO1-Q68H* (Fig. 2I) in Y1469 (wt) cells, respectively. Experiments corresponding to comparisons of R276 (wt) cells versus mutant cells are as follows: *sst2*Δ, 21; *rst1*Δ *rst2*Δ, 22; *fus3*Δ, 32; *bni1*Δ, 34; *fus3*Δ *kss1*Δ, 38; *ste7*Δ, 39; *ste12*Δ, 40; *ste18*Δ, 41; *ste4*Δ, 42; *ste5*Δ, 43; *ste11*Δ, 44. Experiments corresponding to treatments of mutants with 50 nM α-factor for 30 min are as follows: *kss1*Δ, 8; *fus3*Δ, 19; *far1*Δ, 20; *ste20*Δ, 29; *rst1*Δ *rst2*Δ, 30; *fus3-K42R*, 31. Direct comparisons of wt versus mutant strains, both of which were treated with 50 nM α-factor, identified genes induced or repressed specifically in the mutant strain, as follows: R276 (wt) versus *fus3*Δ (30 min), 33; R276 (wt) versus *tec1*Δ (30 min), 45; R276 (wt) versus *tec1*Δ (120 min), 46. Experiment 23 involved treating *hog1*Δ cells with 1 M sorbitol for 2 hours.
34. Supported by Rosetta Inpharmatics, and grants to C.B. from the Natural Sciences and Engineering Research Council of Canada and the National Cancer Institute of Canada. We thank G. Fink, L. Hartwell, I. Herskowitz, H. Madhani, P. Pryciak, and S. O'Rourke for plasmids and yeast strains; F. Naider for synthetic **a**-factor; T. R. Ward and S. Whelen for yeast strains; K. Kennedy and A. Tong for assistance with β-galactosidase experiments and figures; and M. Ashby, A. Breitkreutz, H. Bussey, N. Davis, L. Harrington, L. Hartwell, P. Pryciak, J. Rine, T. Roemer, and P. Young for comments on the manuscript.

14 July 1999; accepted 15 December 1999